Searching for double-peak and doubly broken gravitational-wave spectra from Advanced LIGO-Virgo's first three observing runs

Wang-Wei Yu [1,2,*] and Shao-Jiang Wang [1,†]

[1] *CAS Key Laboratory of Theoretical Physics, Institute of Theoretical Physics, Chinese Academy of Sciences, Beijing 100190, China*

[2] *School of Physical Sciences, University of Chinese Academy of Sciences (UCAS), Beijing 100049, China*

(Received 11 December 2022; revised 23 June 2023; accepted 5 September 2023; published 27 September 2023)

The current LIGO-Virgo observing run has been pushing the sensitivity limit to touch the stochastic gravitational-wave backgrounds (SGWBs). However, no significant detection has been reported to date for any single dominated source of SGWBs with a single broken-power-law (BPL) spectrum. Nevertheless, it could equally well escape from existing Bayesian searches from, for example, two comparable dominated sources with two separate BPL spectra (double-peak case) or a single source with its power-law behavior in the spectrum broken twice (doubly broken case). In this paper, we put constraints on these two cases but specifically for the model with cosmological first-order phase transitions from Advanced LIGO-Virgo's first three observing runs. We found strong negative evidence for the double-peak case and hence place 95% confidential level (CL) upper limits $\Omega_{\mathrm{BPL},1} < 5.8 \times 10^{-8}$ and $\Omega_{\mathrm{BPL},2} < 4.4 \times 10^{-8}$ on the two BPL spectra amplitudes with respect to the unresolved compact binary coalescence (CBC) amplitude $\Omega_{\mathrm{CBC}} < 5.6 \times 10^{-9}$. We further found weak negative evidence for the doubly broken case and hence place 95% CL upper limit $\Omega_{\mathrm{DB}} < 1.2 \times 10^{-7}$ on the overall amplitude of the doubly broken spectrum with respect to $\Omega_{\mathrm{CBC}} < 6.0 \times 10^{-9}$. In particular, the results from the double-peak case have marginally ruled out the strong super-cooling first-order phase transitions at LIGO-Virgo band.

DOI: 10.1103/PhysRevD.108.063526

I. INTRODUCTION

The sensitivity limits have been persistently pushed forward during the first three observing runs (O1 [1], O2 [2], and O3 [3]) of the Advanced LIGO [4] and Advanced Virgo [5] gravitational wave (GW) detectors, which might uncover the stochastic GW backgrounds (SGWBs) [6–8] from unresolved sources of both astrophysical and cosmological origins. The unresolved sources of astrophysical origins mainly consist of the compact binary coalescences (CBCs) from unresolved individual sources such as binary black hole and neutron star mergers [9–13] as well as other more exotic sources that are also more difficult to be observed, including the core-collapse supernovae [14–17], rotating neutron stars [18–24], stellar-core collapses [25–27], and boson clouds around black holes [28–34], to name just a few.

The SGWBs of cosmological origins [35] can embrace much more rich physics [36,37]. Primordial GWs produced from an inflationary era [38] uniquely mark the energy scale of cosmic inflation, in particular, the scalar-induced secondary GWs [39–43] during inflation depict the curvature perturbations at small scales. The SGWBs from cosmological first-order phase transitions (FOPTs) [44–48] and cosmic strings [49–52] necessarily encode the new physics beyond the standard model of particle physics, while the SGWBs from primordial black hole (PBH) mergers [53] can constrain the PBH abundance in the dark matter. However, multiple sources of these SGWBs of cosmological origins can be equally well present simultaneously in the GW data.

The detectability for SGWBs below the confusion limit is by no doubt difficult compared to the individually resolvable GW events that make up a tiny fraction of all GW signals present in the detector time stream. The most recent isotropic search [54] from O3 combined with previous ones from O1 [55] and O2 [56] is consistent with uncorrelated noise and hence places upper limits on the normalized GW energy density for power-law spectral-index values of 0 (flat), 2/3 (CBCs), and 3 (causality). Other efforts of searches with LIGO-Virgo Collaboration for the SGWBs from cosmic strings [57,58], FOPTs [59–62], and induced GWs [63,64] all return a null result.

However, a simple Bayesian search with a single broken power-law (BPL) spectrum for any single but dominated source of SGWBs might just miss possible detections on, for example, two comparable dominated sources of SGWBs with two separate single-BPL spectra (double-peak case) or a single source of SGWBs with its power-law

*yuwangwei@mail.itp.ac.cn

†Corresponding author: schwang@itp.ac.cn

 © 2023 American Physical Society

behavior in the spectrum broken twice (double-broken case). The double-peak (DP) case also includes a single source of SGWBs but already with two peaks by nature, for example, two-step FOPT [65,66], one-step FOPT but with comparable GWs from both wall collisions and sound waves when bubbles collide during the transition to a near constant terminal wall velocity [67], induced GWs with two peaks for some particular configuration on curvature perturbations [68], oscillons with cuspy potentials [69] during preheating era. The doubly broken (DB) case can be found in an analytic evaluation on the GWs from wall collisions beyond the envelope approximation [70] and a hybrid simulation for the sound waves [71] (see also [72]).

In this paper, we search for the SGWB signals in the cases with DP and DB spectra from Advanced LIGO-Virgo's first three observing runs but with a special focus on SGWBs from FOPTs. The models are introduced in Sec. II and constrained in Sec. III, and the results are summarized in Sec. IV.

II. MODELS

The BPL spectrum of SGWBs can be modeled as

$$\Omega_{\rm BPL}(f;\boldsymbol{\theta}) = \Omega_* \left(\frac{f}{f_*}\right)^{n_1} \left[\frac{1+(f/f_*)^{\Delta}}{2}\right]^{(n_2-n_1)/\Delta} \quad (1)$$

with $\boldsymbol{\theta} \equiv (\Omega_*, f_*, n_1, n_2, \Delta)$, where Ω_* is the peak amplitude at the peak frequency f_*, n_1 ($=3$ for causality) and n_2 are the asymptotic slopes on the far left and far right ends of the peak frequency, respectively, and $1/\Delta$ is the peak transition width. We define the DP spectrum as simply the sum of two separate BPL spectra,

$$\Omega_{\rm DP}(f;\{\boldsymbol{\theta}_1,\boldsymbol{\theta}_2\}) = \Omega_{\rm BPL}(f;\boldsymbol{\theta}_1) + \Omega_{\rm BPL}(f;\boldsymbol{\theta}_2) \quad (2)$$

with $\boldsymbol{\theta}_i \equiv (\Omega_{*,i}, f_{*,i}, n_{1,i}, n_{2,i}, \Delta_i)$ for the peaks $i = 1, 2$, while the DB spectrum is modeled as a three-section power-law scaling by

$$\Omega_{\rm DB}(f;\boldsymbol{\theta}) = \frac{\Omega_*}{\left(\frac{f}{f_l}\right)^{-n_l} + \left(\frac{f}{f_l}\right)^{-n_m} + \left(\frac{f_h}{f_l}\right)^{-n_m}\left(\frac{f}{f_h}\right)^{-n_h}} \propto \begin{cases} (f/f_l)^{n_l}, & f \ll f_l, \\ (f/f_l)^{n_m}, & f_l \ll f \ll f_h, \\ (f_h/f_l)^{n_m}(f/f_h)^{n_h}, & f_h \ll f, \end{cases} \quad (3)$$

with $\boldsymbol{\theta} \equiv (\Omega_*, f_l, f_h, n_l, n_m, n_h)$, where we will assume $n_l > n_m > n_h$ and $f_l < f_h$ with a specific example [71] in mind. An explicit comparison between DP and DB spectra is shown in Fig. 1. The reference SGWBs from unresolved CBCs can be approximated by a $f^{2/3}$ power-law spectrum [73] in the inspiral phase as

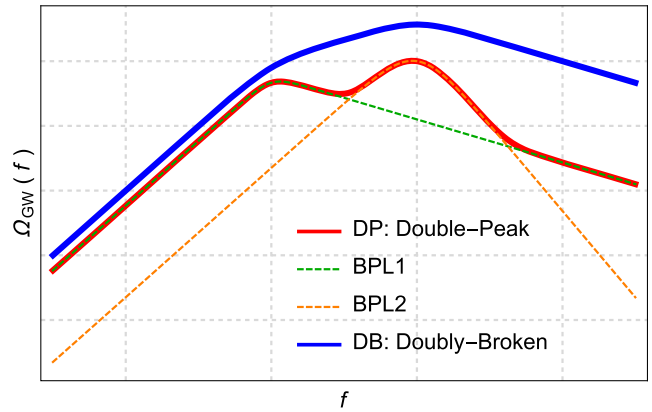

FIG. 1. The schematic comparison between DP (red solid) and DB (blue solid) spectra for the SGWB. The DP spectrum consists of two separate BPL spectra (green and orange dashed) while the DB spectrum admits a three-section power-law scaling.

$$\Omega_{\rm CBC}(f;\boldsymbol{\theta}) = \Omega_{\rm ref}\left(\frac{f}{f_{\rm ref}}\right)^{2/3} \quad (4)$$

with $\boldsymbol{\theta} \equiv (\Omega_{\rm ref}, f_{\rm ref})$, where $\Omega_{\rm ref}$ is the reference amplitude at the reference frequency $f_{\rm ref}$ that will be fixed at 25 Hz around the most sensitive frequency band of the LIGO-Virgo network. For all the above models, the uncorrelated Gaussian noise is implicitly included with $\Omega_{\rm N}(f) = 0$.

The primary motivation to test above models beyond the simple BPL model comes from SGWBs from FOPTs, which usually occur for breaking some continuous symmetry that would form a potential barrier for the false vacuum decaying into the true vacuum. The vacuum decay process proceeds via spontaneous nucleations of true vacuum bubbles in the false vacuum plasma, followed by rapid expansions of bubble walls until violent collisions, along with which the expanding bubble walls also stimulate fluid motions of the thermal plasma. Therefore, both the bubble wall collisions and plasma fluid motions would generate SGWBs. The simple BPL spectrum with $n_1 = 3$, $n_2 = -1$, and $\Delta = 4$ can depicts the GW spectrum from bubble-wall collisions under the dubbed envelope approximation [74], in which case the overlapping parts of thin walls are neglected upon collisions. However, by going beyond the envelope approximation, the analytic modeling [70] of wall collisions reveals a three-section power-law scaling with $n_l = 3$, $n_m = 1$, and $n_h = -1$ that can be described by a DB spectrum. Furthermore, the GWs from plasma fluid motions especially the dominated contributions from sound waves can also be fitted by the simple BPL spectrum with $n_1 = 3$, $n_2 = -4$, and $\Delta = 2$ as

suggested by numerical simulations [75–77]. However, analytic modelings [78–80] seem to prefer a DB spectrum with $n_l = 3$, $n_m = 1$, and $n_h = -3$ but still with some uncertainty in determining its high-frequency slope within $-3 \leq n_h \leq -1$ [80]. Nevertheless, we will stick to the fitting spectrum from numerical simulation instead of the analytic estimation for the sound waves. On the other hand, it is probable for some specific particle physics model of FOPT in its particular parameter space that the contributions from the envelope collisions and sound waves are comparable, which can be described by a DP spectrum.

III. DATA ANALYSIS

We closely follow the method outlined in Refs. [54,59,63] to search for SGWBs in the current GW data. The log-likelihood for the model parameter set $\boldsymbol{\theta}$ is estimated by [81–84]

$$\log p(\hat{C}_{IJ}|\boldsymbol{\theta}, \lambda) \propto -\frac{1}{2}\sum_k \frac{[\hat{C}_{IJ}(f_k) - \lambda\Omega_{\rm GW}(f_k;\boldsymbol{\theta})]^2}{\sigma^2_{IJ}(f_k)} \tag{5}$$

with the sum k running over the frequency bins, where $\hat{C}_{IJ}(f)$ is the cross-correlation statistic for the baseline IJ with $I, J = H, L, V$ for the LIGO-Hanford, LIGO-Livingston, and Virgo (HLV) detectors, $\sigma^2_{IJ}(f)$ is the variance of $\hat{C}_{IJ}(f)$ in the small signal-to-noise ratio limit [85], and λ accounts for the calibration uncertainties of the detectors [86] that would be eventually marginalized over [87]. Since the current data still favors a pure Gaussian noise model [54], the contribution from Schumann resonances is negligible [83,88,89]. The final likelihood is obtained by summing over multiple log-likelihoods for different baselines in order to constrain the model parameters. As the SGWB from CBCs is an indispensable part of any SGWBs at the LIGO-Virgo band, we will search for SGWBs specifically from FOPTs for the combined models BPL + CBC, DP + CBC, and DB + CBC with their parameter priors depicted in Table I. For model comparison, we adopt the ratios of evidence $\log \mathcal{B}^{i+\rm CBC}_{\rm Noise}$ and $\log \mathcal{B}^{i+\rm CBC}_{\rm CBC}$ from the Bayes factor to evaluate the preference for a specific SGWB model over a pure Gaussian noise model and a CBC background, respectively.

IV. RESULTS

The Bayes-ratio comparison of models constrained by the dynamic nested sampling package DYNESTY [90] in Bilby [91] is summarized in Fig. 2, which will be described in details shortly below. The general conclusion is that, the SGWB from a DP spectrum is even more disfavored than the SGWB with a single BPL spectrum or a DB spectrum, but all of which are not detected compared to the backgrounds from either uncorrelated Gaussian noises or CBCs.

TABLE I. The prior choices for the combined SGWB models BPL + CBC, DP + CBC, and DB + CBC.

BPL + CBC		
Parameter	Prior	
$\Omega_{\rm ref}$	Log-uniform $(10^{-10}, 10^{-7})$	
Ω_*	Log-uniform $(10^{-9}, 10^{-4})$	
f_*	Uniform (0, 256) Hz	
n_1	3	
	Sound waves	Envelope-wall collisions
n_2	−4	−1
Δ	2	4

DP + CBC		
Parameter	Prior	
$\Omega_{\rm ref}$	Log-uniform $(10^{-10}, 10^{-7})$	
$\Omega_{*,i}$	Log-uniform $(10^{-9}, 10^{-4})$	
$f_{*,1}$	Uniform (0, 256) Hz	
$f_{*,2}(> f_{*,1})$	Uniform (0, 256) Hz	
$n_{1,i}$	3	
$n_{2,1}$	−1	Envelope-wall collisions
$n_{2,2}$	−4	Sound waves
Δ_1	4	Envelope-wall collisions
Δ_2	2	Sound waves

DB + CBC		
Parameter	Prior	
$\Omega_{\rm ref}$	Log-uniform $(10^{-10}, 10^{-7})$	
Ω_*	Log-uniform $(10^{-9}, 10^{-4})$	
f_l	Uniform (0, 256) Hz	
$f_h(> f_l)$	Uniform (0, 256) Hz	
$n_l(> n_m)$	3	Beyond envelope-wall collisions
$n_m(> n_h)$	1	
n_h	−1	

A. The BPL + CBC model

To compare with previous results in the literature, we repeat the BPL model of Ref. [59] but with an extra 2 factor in (1) so that Ω_* is exactly the peak amplitude at the peak frequency f_*, while in Ref. [59] the peak amplitude is actually $\Omega_{\rm BPL}(f_*) = 2^{(n_2-n_1)/\Delta}\Omega_*$ instead of Ω_*. For $n_2 < 0 < n_1$ and $\Delta > 0$, the upper bound $\Omega_* = 5.6 \times 10^{-7}$ obtained in Ref. [59] with fixed $n_1 = 3$ and $\Delta = 2$ actually overestimates the true peak amplitude with a larger overestimation for steeper slopes (larger $|n_1|$ and/or $|n_2|$) or a wider transition width (a smaller Δ) around the peak position.

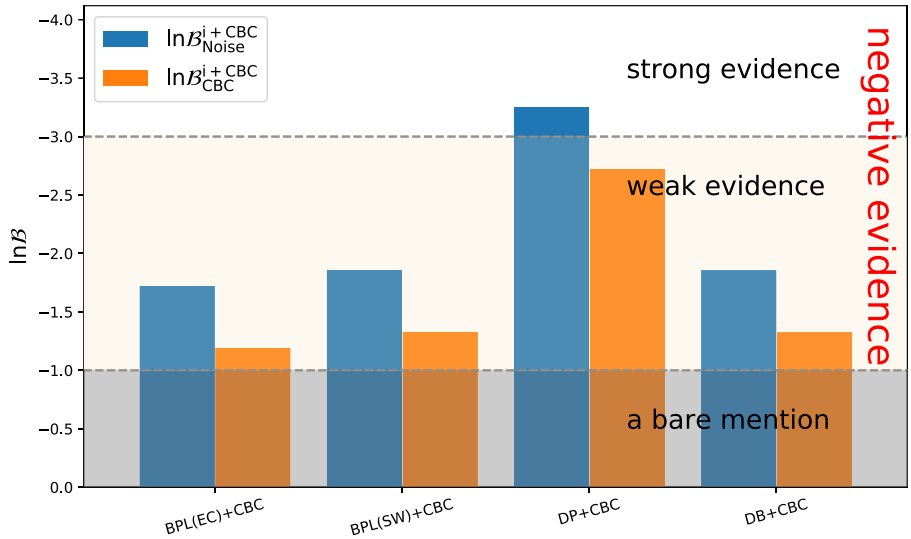

FIG. 2. The Bayes ratios for model comparisons among BPL + CBC models with priors fixed by envelope collisions (EC) and sound waves (SW), DP + CBC model (envelope collisions + sound waves), and DB + CBC model (wall collisions beyond envelope approximation).

In fact, with fixed $n_1 = 3, n_2 = -1$ ($n_2 = -4$), and $\Delta = 4$ ($\Delta = 2$) for SGWBs from envelope collisions (sound waves), the 95% upper limit we found on the peak amplitude reads $\Omega_* < 9.7 \times 10^{-8}$ ($\Omega_* < 8.2 \times 10^{-8}$), which, along with posterior sample of f_* from the Fig. 4, can be combined into a posterior of $\Omega_{\rm BPL}$, leading to a 95% CL constraint $\Omega_{\rm BPL}(25\ {\rm Hz}) < 3.5 \times 10^{-9}$ ($\Omega_{\rm BPL}(25\ {\rm Hz}) < 6.4 \times 10^{-9}$) at the CBC reference frequency $f_* = 25$ Hz, while the CBC reference amplitude is found to be bounded by $\Omega_{\rm ref} < 5.9 \times 10^{-9}$ ($\Omega_{\rm ref} < 5.9 \times 10^{-9}$). The Bayes ratios $\log \mathcal{B}^{\rm BPL+CBC}_{\rm Noise} = -1.72$ ($\log \mathcal{B}^{\rm BPL+CBC}_{\rm Noise} = -1.86$) and $\log \mathcal{B}^{\rm BPL+CBC}_{\rm CBC} = -1.19$ ($\log \mathcal{B}^{\rm BPL+CBC}_{\rm CBC} = -1.33$) even more disfavor a BPL GW spectrum from envelope collisions (sound waves) over SGWBs from either pure Gaussian noises or CBCs than Ref. [59], slightly improving the previous result.

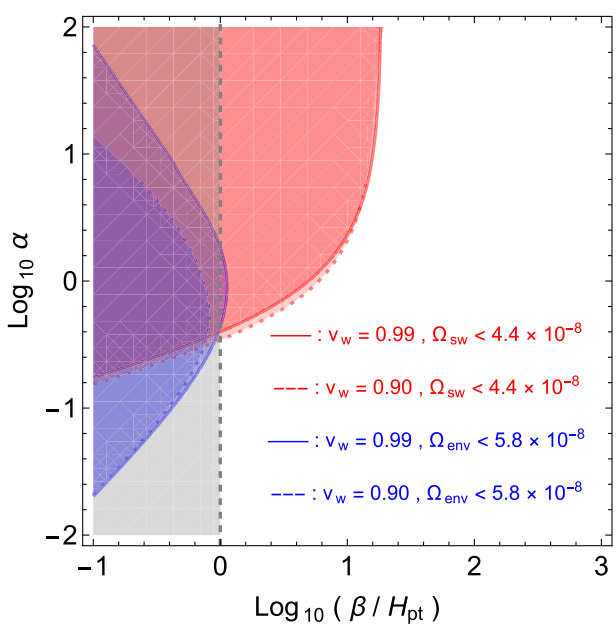

FIG. 3. The implied constraints on the FOPT parameters $\beta/H_{\rm pt}$ and α for the bubble-wall velocities $v_w = 0.9$ (dashed) and $v_w = 0.99$ (solid) from the constraints on the DP + CBC model. The blue and red shaded regions are ruled out by the upper bounds on the low-frequency and high-frequency peak amplitudes, respectively. The gray-shaded region is usually not considered for the FOPT to complete successfully.

B. The DP + CBC model

For the SGWBs from FOPTs, the present peak frequency of envelope collisions [74,92–98],

$$f_{\rm env} = 16.5\left(\frac{f_{\rm bc}}{\beta}\right)\left(\frac{\beta}{H_{\rm pt}}\right)\left(\frac{T_{\rm pt}}{100\ {\rm GeV}}\right)\left(\frac{g_*}{100}\right)^{\frac{1}{6}}\ \mu{\rm Hz} < 5.775\left(\frac{\beta}{H_{\rm pt}}\right)\left(\frac{T_{\rm pt}}{100\ {\rm GeV}}\right)\left(\frac{g_*}{100}\right)^{\frac{1}{6}}\ \mu{\rm Hz}, \tag{6}$$

is always smaller than the present peak frequency of sound waves [75–77,99],

$$f_{\rm sw} = \frac{19}{v_w}\left(\frac{\beta}{H_{\rm pt}}\right)\left(\frac{T_{\rm pt}}{100\ {\rm GeV}}\right)\left(\frac{g_*}{100}\right)^{\frac{1}{6}}\ \mu{\rm Hz} > 19\left(\frac{\beta}{H_{\rm pt}}\right)\left(\frac{T_{\rm pt}}{100\ {\rm GeV}}\right)\left(\frac{g_*}{100}\right)^{\frac{1}{6}}\ \mu{\rm Hz}, \tag{7}$$

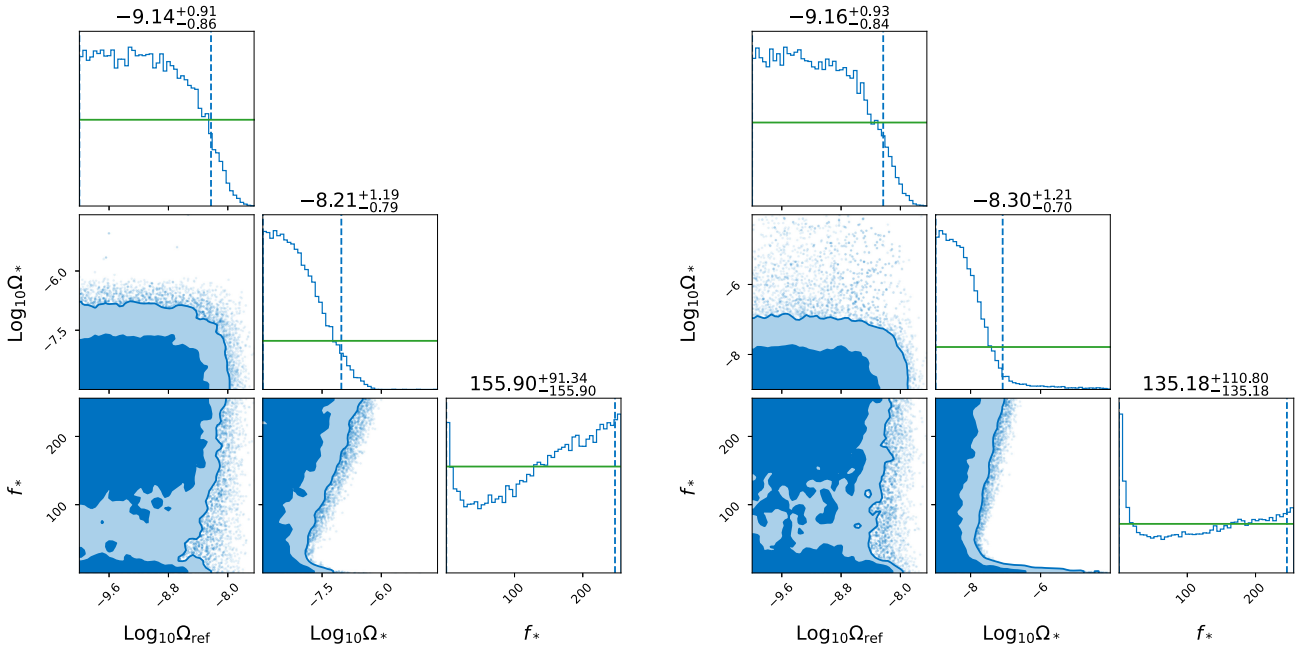

FIG. 4. The parameter posteriors for the BPL + CBC model with BPL priors fixed by envelope collisions (left) and sound waves (right). The 68% and 95% contours are depicted in colors. The vertical dashed lines describe the 95% and the horizon lines are the prior distributions. We also show the (0, 95%) of parameters individually.

for the bubble-wall velocity $0 < v_w < 1$, where $f_{\mathrm{bc}} = 0.35\beta/(1 + 0.069v_w + 0.69v_w^4) < 0.35\beta$ is the peak frequency of bubble collisions right after the phase transition, β/H_{pt} is the Hubble time scale H_{pt}^{-1} relative to the PT duration β^{-1} at the PT temperature T_{pt}, and g_* is the effective number of relativistic degrees of freedom. Therefore, we can specifically fix the priors $f_{*,1} < f_{*,2}$ with $n_{2,1} = -1$, $\Delta_1 = 4$ (envelope collisions) and $n_{2,2} = -4$, $\Delta_2 = 2$ (sound waves) as well as $n_{1,i} = 3$ (by causality) for both $i = 1$ (envelope collisions) and $i = 2$ (sound waves), and then place 95% CL upper limits on the low-frequency peak amplitude $\Omega_{*,1} < 5.8 \times 10^{-8}$ and high-frequency peak amplitude $\Omega_{*,2} < 4.4 \times 10^{-8}$, while the CBC reference amplitude is bounded by $\Omega_{\mathrm{ref}} < 5.6 \times 10^{-9}$ as obtained from Fig. 5. The Bayes ratios $\log \mathcal{B}_{\mathrm{Noise}}^{\mathrm{DP+CBC}} = -3.25$ and $\log \mathcal{B}_{\mathrm{CBC}}^{\mathrm{DP+CBC}} = -2.72$ strongly disfavor for the DP + CBC over either noises or CBCs than the single BPL + CBC model does.

The above constraints on the low-frequency and high-frequency peak amplitudes can be transformed into constraints on the PT inverse duration β/H_{pt} and strength factor α for a given bubble-wall velocity v_w. The peak amplitude of envelope collisions is known as [74,92–98]

$$\Omega_{\mathrm{env}} = 1.67 \times 10^{-5} \frac{A}{h^2} \left(\frac{H_{\mathrm{pt}}}{\beta}\right)^2 \left(\frac{\kappa_\phi \alpha}{1+\alpha}\right)^2 \left(\frac{100}{g_*}\right)^{\frac{1}{3}}, \quad (8)$$

where $A(v_w) \equiv 0.48 v_w^3/(1 + 5.3v_w^2 + 5v_w^4)$ is the amplitude and κ_ϕ is the efficiency factor of inserting released vacuum energy into the bubble wall kinetic energy evaluated generally in Ref. [67]. For the most optimistic constraint, we can take a crude estimation $\kappa_\phi \approx 1 - \kappa_{\mathrm{sw}}$ from the efficiency factor κ_{sw} of fluid motions given shortly below. The peak amplitude of sound waves is known as [75–77,99]

$$\Omega_{\mathrm{sw}} = 2.65 \times 10^{-6} \frac{v_w}{h^2} \left(\frac{H_{\mathrm{pt}}}{\beta}\right) \left(\frac{\kappa_{\mathrm{sw}} \alpha}{1+\alpha}\right)^2 \left(\frac{100}{g_*}\right)^{\frac{1}{3}} \Upsilon, \quad (9)$$

where the efficiency factor $\kappa_{\mathrm{sw}}(\alpha, v_w)$ of bulk fluid motions can be fitted as a function of α and v_w by hydrodynamics [100] (see also [101] for the varying sound velocity generalization to the constant sound velocity estimations [102–104]). The suppression factor $\Upsilon \equiv 1 - (1 + 2\tau_{\mathrm{sw}} H_{\mathrm{pt}})^{-1/2}$ [105] accounts for the finite lifetime of sound waves from the onset timescale of turbulence, $\tau_{\mathrm{sw}} H_{\mathrm{pt}} \approx (8\pi)^{1/3} v_w/(\beta/H_{\mathrm{pt}})/\bar{U}_f$, with the root-mean-squared fluid velocity given by $\bar{U}_f^2 = 3\kappa_{\mathrm{sw}}\alpha/[4(1+\alpha)]$ [106]. In all cases, we can take the effective number of degrees of freedom $g_* = 100$ and dimensionless Hubble constant $h = 0.67$ for illustration. Therefore, both peak amplitudes Ω_{env} and Ω_{sw} can be expressed for a given v_w as functions of β/H_{pt} and α, which can be further constrained in Fig. 3 with the blue and red shaded regions ruled out by $\Omega_{\mathrm{env}} = \Omega_{*,1} < 5.8 \times 10^{-8}$ and $\Omega_{\mathrm{sw}} = \Omega_{*,2} < 4.4 \times 10^{-8}$,

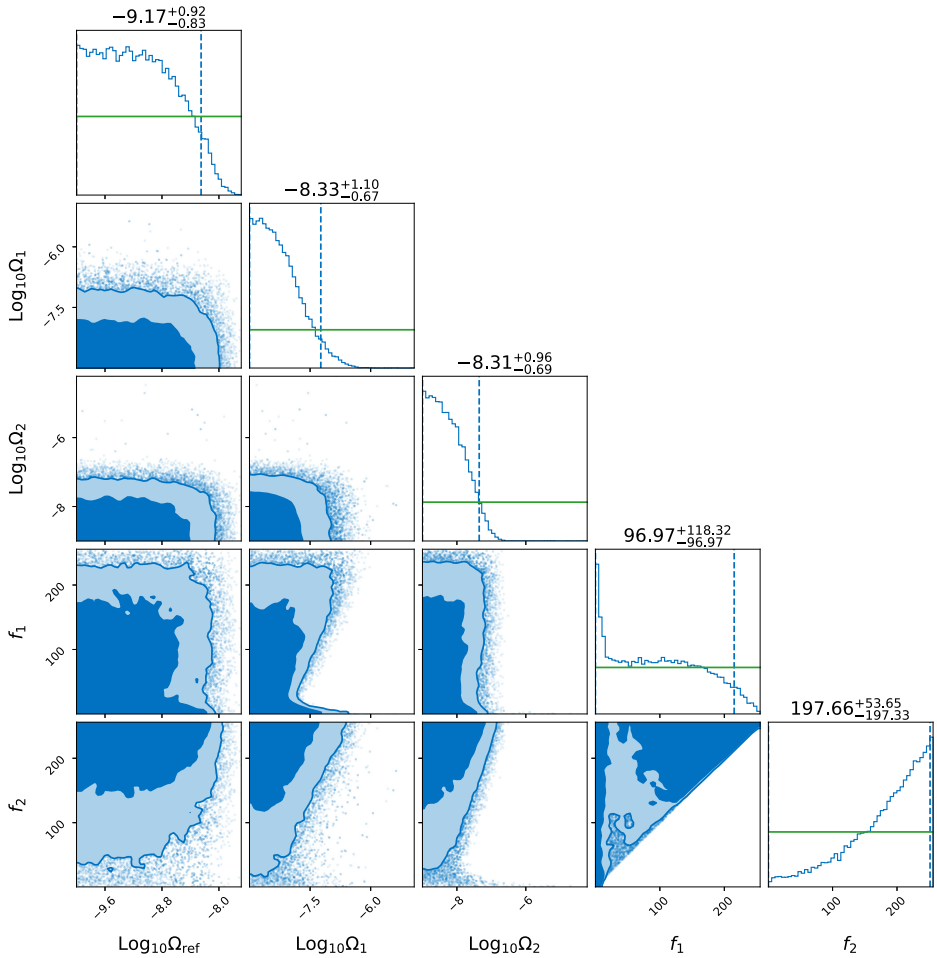

FIG. 5. The parameter posteriors for the BP (envelope collisions + sound waves) +CBC model. The 68% and 95% contours are depicted in colors. The vertical dashed lines describe the 95% and the horizon lines are the prior distributions. We also show the (0, 95%) of parameters individually.

respectively. Although the current GW data cannot put strong constraints on the FOPTs, the very strong FOPTs of super-cooling type in the LIGO-Virgo band with $\alpha \gtrsim \mathcal{O}(1)$ and $\beta/H_{\mathrm{pt}} \lesssim \mathcal{O}(10)$ can be marginally ruled out from Fig. 3. Note here that there is no precise but conventional definition [107] for the very strong FOPT of super-cooling type. The strength factor α measures the relative size of released vacuum energy density with respect to the background radiation energy density, and hence $\alpha \gtrsim \mathcal{O}(1)$ indicates a very strong FOPT. The other parameter β/H_{pt} measures the relative size of Hubble horizon scale H_{pt}^{-1} with respect to the mean bubble separation $(8\pi)^{1/3} v_w \beta^{-1} \sim \beta^{-1}$, and hence $\beta/H_{\mathrm{pt}} \lesssim \mathcal{O}(10)$ indicates a relatively large radius of bubbles at collisions, which would result in a relatively long PT duration [108,109] that leads to ultra-low temperature at percolations than the critical/nucleation temperature (hence the name super cooling).

C. The DB + CBC model

For a physical process associated with two characteristic length scales, the generated SGWBs usually admit a doubly broken (DB) power-law spectrum. One such example is the cosmological FOPT with the vacuum-bubble collisions characterized by the averaged initial bubble separation and bubble-wall thickness, and sound waves characterized by the averaged initial bubble separation and sound shell thickness [71,78–80]. We consider specifically in this section the GWs from the bubble-wall collisions beyond the envelope approximation with $n_l = 3$, $n_m = 1$, and $n_h = -1$. The overall amplitude can be constrained as $\Omega_* < 1.2 \times 10^{-7}$, which, after combined with the posterior samples of f_l, and f_h in Fig. 6, renders 95% CL upper bound $\Omega_{\mathrm{DB}}(25\ \mathrm{Hz}) < 2.3 \times 10^{-9}$ at the CBC reference frequency with the corresponding CBC reference amplitude bounded by $\Omega_{\mathrm{ref}} < 6.0 \times 10^{-9}$. Similar to the single BPL + CBC

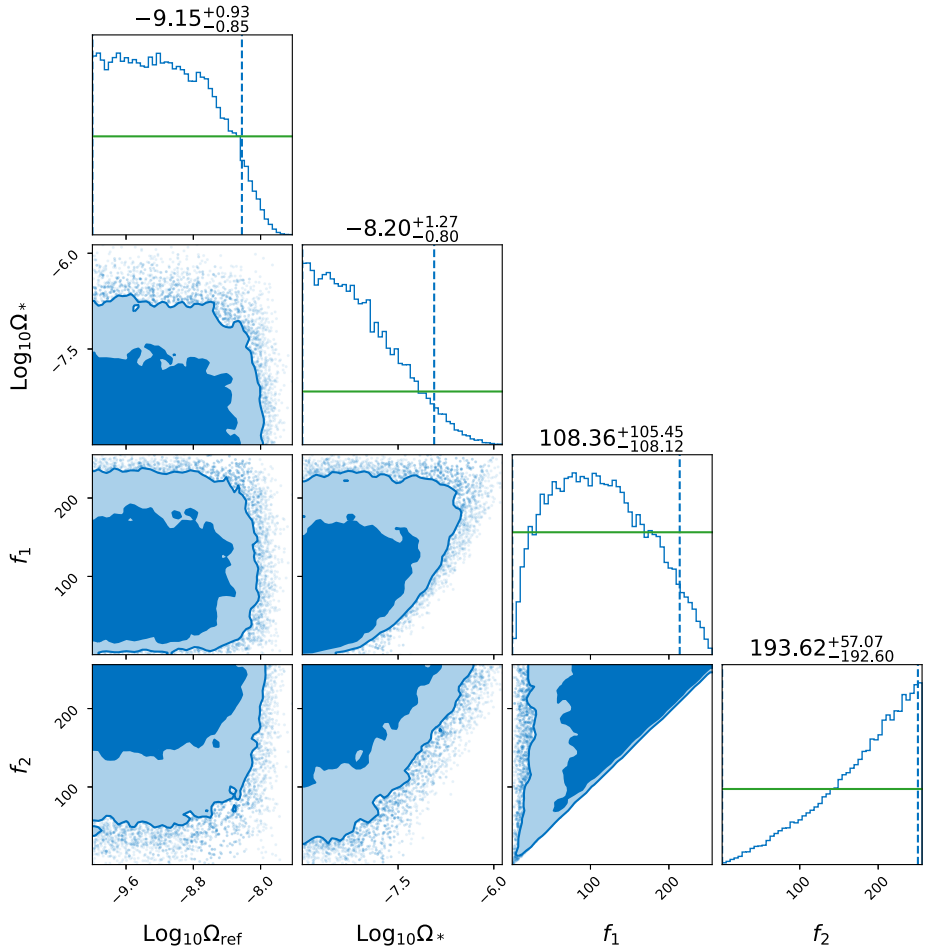

FIG. 6. The parameter posteriors for the DB (beyond envelope) + CBC model. The 68% and 95% contours are depicted in colors. The vertical dashed lines describe the 95% and the horizon lines are the prior distributions. We also show the (0, 95%) of parameters individually.

model, the Bayes ratios $\log \mathcal{B}^{\mathrm{DBPL+CBC}}_{\mathrm{Noise}} = -1.86$ and $\log \mathcal{B}^{\mathrm{DB+CBC}}_{\mathrm{CBC}} = -1.33$ also slightly disfavor for the DB + CBC over either noises or CBCs.

V. CONCLUSIONS AND DISCUSSIONS

In this paper, we have implemented the Bayes search for the SGWBs specifically from the cosmological first-order phase transitions with a DP or DB spectrum in the first three observing runs of the Advanced LIGO-Virgo collaborations. No positive evidence has been found for both DP + CBC and DB + CBC models with respective to the backgrounds from either Gaussian noises or CBCs, though the DP + CBC is even more disfavored than the DB + CBC model as well as the usual BPL + CBC model. In particular, our results for the BPL + CBC model slightly improve the previous claim on the null detection for the BPL spectrum, and the DP + CBC results motivated from FOPTs could marginally rule out the very strong FOPT of super-cooling type in the LIGO-Virgo band. All these results could be further improved for the upcoming fourth observing run of the LIGO/Virgo/KAGRA Collaboration, but currently we are still on the way to uncover the SGWBs.

ACKNOWLEDGMENTS

We thank Huai-Ke Guo, Katarina Martinovic, and Alba Romero for fruitful correspondence on the calibration uncertainties in the LIGO/VIRGO analysis. We thank the helpful discussion on the code with Wen-Hong Ruan, Chang Liu, and He Wang. This work is supported by the National Key Research and Development Program of China Grants No. 2021YFC2203004, No. 2021YFA0718304, and No. 2020YFC2201501, the National Natural Science Foundation of China Grants No. 12105344, No. 12235019, and No. 12047503, the Key Research Program of the Chinese Academy of Sciences (CAS) Grant No. XDPB15, the Key Research Program of Frontier Sciences of CAS, and the Science Research Grants from the China Manned Space Project No. CMS-CSST-2021-B01. We also acknowledge the use of the HPC Cluster of ITP-CAS.

[1] B. P. Abbott *et al.* (LIGO Scientific and Virgo Collaborations), GWTC-1: A Gravitational-Wave Transient Catalog of Compact Binary Mergers Observed by LIGO and Virgo During the First and Second Observing Runs, Phys. Rev. X **9**, 031040 (2019).
[2] R. Abbott *et al.* (LIGO Scientific and Virgo Collaborations), GWTC-2: Compact Binary Coalescences Observed by LIGO and Virgo During the First Half of the Third Observing Run, Phys. Rev. X **11**, 021053 (2021).
[3] R. Abbott *et al.* (LIGO Scientific, Virgo, and KAGRA Collaborations), GWTC-3: Compact Binary Coalescences Observed by LIGO and Virgo During the Second Part of the Third Observing Run, arXiv:2111.03606 [Phys. Rev. X (to be published)].
[4] J. Aasi *et al.* (LIGO Scientific Collaborations), Advanced LIGO, Classical Quantum Gravity **32**, 074001 (2015).
[5] F. Acernese *et al.* (Virgo Collaborations), Advanced Virgo: A second-generation interferometric gravitational wave detector, Classical Quantum Gravity **32**, 024001 (2015).
[6] N. Christensen, Stochastic gravitational wave backgrounds, Rep. Prog. Phys. **82**, 016903 (2019).
[7] A. I. Renzini, B. Goncharov, A. C. Jenkins, and P. M. Meyers, Stochastic gravitational-wave backgrounds: Current detection efforts and future prospects, Galaxies **10**, 34 (2022).
[8] N. van Remortel, K. Janssens, and K. Turbang, Stochastic gravitational wave background: Methods and Implications, Prog. Part. Nucl. Phys. **128**, 104003 (2023).
[9] P. A. Rosado, Gravitational wave background from binary systems, Phys. Rev. D **84**, 084004 (2011).
[10] X.-J. Zhu, E. Howell, T. Regimbau, D. Blair, and Z.-H. Zhu, Stochastic gravitational wave background from coalescing binary black holes, Astrophys. J. **739**, 86 (2011).
[11] S. Marassi, R. Schneider, G. Corvino, V. Ferrari, and S. Portegies Zwart, Imprint of the merger and ring-down on the gravitational wave background from black hole binaries coalescence, Phys. Rev. D **84**, 124037 (2011).
[12] C. Wu, V. Mandic, and T. Regimbau, Accessibility of the gravitational-wave background due to binary coalescences to second and third generation gravitational-wave detectors, Phys. Rev. D **85**, 104024 (2012).
[13] X.-J. Zhu, E. J. Howell, D. G. Blair, and Z.-H. Zhu, On the gravitational wave background from compact binary coalescences in the band of ground-based interferometers, Mon. Not. R. Astron. Soc. **431**, 882 (2013).
[14] A. Buonanno, G. Sigl, G. G. Raffelt, H.-T. Janka, and E. Muller, Stochastic gravitational wave background from cosmological supernovae, Phys. Rev. D **72**, 084001 (2005).
[15] P. Sandick, K. A. Olive, F. Daigne, and E. Vangioni, Gravitational waves from the first stars, Phys. Rev. D **73**, 104024 (2006).
[16] S. Marassi, R. Schneider, and V. Ferrari, Gravitational wave backgrounds and the cosmic transition from population III to population II stars, Mon. Not. R. Astron. Soc. **398**, 293 (2009).
[17] X.-J. Zhu, E. Howell, and D. Blair, Observational upper limits on the gravitational wave production of core collapse supernovae, Mon. Not. R. Astron. Soc. **409** (2010), L132.
[18] V. Ferrari, S. Matarrese, and R. Schneider, Stochastic background of gravitational waves generated by a cosmological population of young, rapidly rotating neutron stars, Mon. Not. R. Astron. Soc. **303**, 258 (1999).
[19] E. Howell, T. Regimbau, A. Corsi, D. Coward, and R. Burman, Gravitational wave background from sub-luminous GRBs: Prospects for second and third generation detectors, Mon. Not. R. Astron. Soc. **410**, 2123 (2011).
[20] X.-J. Zhu, X.-L. Fan, and Z.-H. Zhu, Stochastic gravitational wave background from neutron star r-mode instability revisited, Astrophys. J. **729**, 59 (2011).
[21] S. Marassi, R. Ciolfi, R. Schneider, L. Stella, and V. Ferrari, Stochastic background of gravitational waves emitted by magnetars, Mon. Not. R. Astron. Soc. **411**, 2549 (2011).
[22] P. A. Rosado, Gravitational wave background from rotating neutron stars, Phys. Rev. D **86**, 104007 (2012).
[23] C.-J. Wu, V. Mandic, and T. Regimbau, Accessibility of the stochastic gravitational wave background from magnetars to the interferometric gravitational wave detectors, Phys. Rev. D **87**, 042002 (2013).
[24] P. D. Lasky, M. F. Bennett, and A. Melatos, Stochastic gravitational wave background from hydrodynamic turbulence in differentially rotating neutron stars, Phys. Rev. D **87**, 063004 (2013).
[25] K. Crocker, V. Mandic, T. Regimbau, K. Belczynski, W. Gladysz, K. Olive, T. Prestegard, and E. Vangioni, Model of the stochastic gravitational-wave background due to core collapse to black holes, Phys. Rev. D **92**, 063005 (2015).
[26] K. Crocker, T. Prestegard, V. Mandic, T. Regimbau, K. Olive, and E. Vangioni, Systematic study of the stochastic gravitational-wave background due to stellar core collapse, Phys. Rev. D **95**, 063015 (2017).
[27] B. Finkel, H. Andresen, and V. Mandic, Stochastic gravitational-wave background from stellar core-collapse events, Phys. Rev. D **105**, 063022 (2022).
[28] R. Brito, S. Ghosh, E. Barausse, E. Berti, V. Cardoso, I. Dvorkin, A. Klein, and P. Pani, Stochastic and Resolvable Gravitational Waves from Ultralight Bosons, Phys. Rev. Lett. **119**, 131101 (2017).
[29] R. Brito, S. Ghosh, E. Barausse, E. Berti, V. Cardoso, I. Dvorkin, A. Klein, and P. Pani, Gravitational wave searches for ultralight bosons with LIGO and LISA, Phys. Rev. D **96**, 064050 (2017).
[30] X.-L. Fan and Y.-B. Chen, Stochastic gravitational-wave background from spin loss of black holes, Phys. Rev. D **98**, 044020 (2018).
[31] L. Tsukada, T. Callister, A. Matas, and P. Meyers, First search for a stochastic gravitational-wave background from ultralight bosons, Phys. Rev. D **99**, 103015 (2019).
[32] C. Palomba *et al.*, Direct Constraints on Ultra-Light Boson Mass from Searches for Continuous Gravitational Waves, Phys. Rev. Lett. **123**, 171101 (2019).
[33] L. Sun, R. Brito, and M. Isi, Search for ultralight bosons in Cygnus X-1 with Advanced LIGO, Phys. Rev. D **101**, 063020 (2020); **102**, 089902(E) (2020).
[34] R. Abbott *et al.* (KAGRA, Virgo, and LIGO Scientific Collaborations), All-sky search for gravitational wave

emission from scalar boson clouds around spinning black holes in LIGO O3 data, Phys. Rev. D **105**, 102001 (2022).
[35] C. Caprini and D. G. Figueroa, Cosmological backgrounds of gravitational waves, Classical Quantum Gravity **35**, 163001 (2018).
[36] R.-G. Cai, Z. Cao, Z.-K. Guo, S.-J. Wang, and T. Yang, The gravitational-wave physics, Natl. Sci. Rev. **4**, 687 (2017).
[37] L. Bian *et al.*, The gravitational-wave physics II: Progress, Sci. China Phys. Mech. Astron. **64**, 120401 (2021).
[38] M. S. Turner, Detectability of inflation produced gravitational waves, Phys. Rev. D **55**, R435 (1997).
[39] K. Nakamura, Second-order gauge invariant cosmological perturbation theory: Einstein equations in terms of gauge invariant variables, Prog. Theor. Phys. **117**, 17 (2007).
[40] K. N. Ananda, C. Clarkson, and D. Wands, The cosmological gravitational wave background from primordial density perturbations, Phys. Rev. D **75**, 123518 (2007).
[41] B. Osano, C. Pitrou, P. Dunsby, J.-P. Uzan, and C. Clarkson, Gravitational waves generated by second order effects during inflation, J. Cosmol. Astropart. Phys. 04 (2007) 003.
[42] D. Baumann, P. J. Steinhardt, K. Takahashi, and K. Ichiki, Gravitational wave spectrum induced by primordial scalar perturbations, Phys. Rev. D **76**, 084019 (2007).
[43] R.-G. Cai, S. Pi, and M. Sasaki, Gravitational Waves Induced by Non-Gaussian Scalar Perturbations, Phys. Rev. Lett. **122**, 201101 (2019).
[44] C. Caprini *et al.*, Science with the space-based interferometer eLISA. II: Gravitational waves from cosmological phase transitions, J. Cosmol. Astropart. Phys. 04 (2016) 001.
[45] A. Mazumdar and G. White, Review of cosmic phase transitions: Their significance and experimental signatures, Rep. Prog. Phys. **82**, 076901 (2019).
[46] C. Caprini *et al.*, Detecting gravitational waves from cosmological phase transitions with LISA: An update, J. Cosmol. Astropart. Phys. 03 (2020) 024.
[47] M. B. Hindmarsh, M. Lüben, J. Lumma, and M. Pauly, Phase transitions in the early universe, SciPost Phys. Lect. Notes **24**, 1 (2021).
[48] R. Caldwell *et al.*, Detection of early-universe gravitational wave signatures and fundamental physics, Gen. Relativ. Gravit. **54**, 156 (2022).
[49] T. W. B. Kibble, Topology of cosmic domains and strings, J. Phys. A **9**, 1387 (1976).
[50] S. Sarangi and S. H. H. Tye, Cosmic string production towards the end of brane inflation, Phys. Lett. B **536**, 185 (2002).
[51] T. Damour and A. Vilenkin, Gravitational radiation from cosmic (super)strings: Bursts, stochastic background, and observational windows, Phys. Rev. D **71**, 063510 (2005).
[52] X. Siemens, V. Mandic, and J. Creighton, Gravitational Wave Stochastic Background from Cosmic (Super)Strings, Phys. Rev. Lett. **98**, 111101 (2007).
[53] S. Wang, Y.-F. Wang, Q.-G. Huang, and T. G. F. Li, Constraints on the Primordial Black Hole Abundance from the First Advanced LIGO Observation Run Using the Stochastic Gravitational-Wave Background, Phys. Rev. Lett. **120**, 191102 (2018).
[54] R. Abbott *et al.* (KAGRA, Virgo, and LIGO Scientific Collaborations), Upper limits on the isotropic gravitational-wave background from Advanced LIGO and Advanced Virgo's third observing run, Phys. Rev. D **104**, 022004 (2021).
[55] B. P. Abbott *et al.* (LIGO Scientific and Virgo Collaborations), Upper Limits on the Stochastic Gravitational-Wave Background from Advanced LIGO's First Observing Run, Phys. Rev. Lett. **118**, 121101 (2017); **119**, 029901(E) (2017).
[56] B. P. Abbott *et al.* (LIGO Scientific and Virgo Collaborations), Search for the isotropic stochastic background using data from Advanced LIGO's second observing run, Phys. Rev. D **100**, 061101 (2019).
[57] B. P. Abbott *et al.* (LIGO Scientific and Virgo Collaborations), Constraints on cosmic strings using data from the first Advanced LIGO observing run, Phys. Rev. D **97**, 102002 (2018).
[58] R. Abbott *et al.* (LIGO Scientific, Virgo, and KAGRA Collaborations), Constraints on Cosmic Strings Using Data from the Third Advanced LIGO–Virgo Observing Run, Phys. Rev. Lett. **126**, 241102 (2021).
[59] A. Romero, K. Martinovic, T. A. Callister, H.-K. Guo, M. Martínez, M. Sakellariadou, F.-W. Yang, and Y. Zhao, Implications for First-Order Cosmological Phase Transitions from the Third LIGO-Virgo Observing Run, Phys. Rev. Lett. **126**, 151301 (2021).
[60] F. Huang, V. Sanz, J. Shu, and X. Xue, LIGO as a probe of dark sectors, Phys. Rev. D **104**, 095001 (2021).
[61] Y. Jiang and Q.-G. Huang, Constraining the gravitational-wave spectrum from cosmological first-order phase transitions using data from LIGO-Virgo first three observing runs, J. Cosmol. Astropart. Phys. 06 (2023) 053.
[62] C. Badger *et al.*, Probing early universe supercooled phase transitions with gravitational wave data, Phys. Rev. D **107**, 023511 (2023).
[63] A. Romero-Rodriguez, M. Martinez, O. Pujolàs, M. Sakellariadou, and V. Vaskonen, Search for a Scalar Induced Stochastic Gravitational Wave Background in the Third LIGO-Virgo Observing Run, Phys. Rev. Lett. **128**, 051301 (2022).
[64] B. Mu, G. Cheng, J. Liu, and Z.-K. Guo, Constraints on ultra-slow-roll inflation from the third LIGO-Virgo observing run, Phys. Rev. D **107**, 043528 (2023).
[65] F. Bigazzi, A. Caddeo, A. L. Cotrone, and A. Paredes, Dark holograms and gravitational waves, J. High Energy Phys. 04 (2021) 094.
[66] Z. Zhao, Y. Di, L. Bian, and R.-G. Cai, Probing the electroweak symmetry breaking history with Gravitational waves, arXiv:2204.04427.
[67] R.-G. Cai and S.-J. Wang, Effective picture of bubble expansion, J. Cosmol. Astropart. Phys. 03 (2021) 096.
[68] R.-G. Cai, S. Pi, S.-J. Wang, and X.-Y. Yang, Resonant multiple peaks in the induced gravitational waves, J. Cosmol. Astropart. Phys. 05 (2019) 013.
[69] J. Liu, Z.-K. Guo, R.-G. Cai, and G. Shiu, Gravitational Waves from Oscillons with Cuspy Potentials, Phys. Rev. Lett. **120**, 031301 (2018).
[70] R. Jinno and M. Takimoto, Gravitational waves from bubble dynamics: Beyond the envelope, J. Cosmol. Astropart. Phys. 01 (2019) 060.

[71] R. Jinno, T. Konstandin, and H. Rubira, A hybrid simulation of gravitational wave production in first-order phase transitions, J. Cosmol. Astropart. Phys. 04 (2021) 014.
[72] R. Jinno, T. Konstandin, H. Rubira, and I. Stomberg, Higgsless simulations of cosmological phase transitions and gravitational waves, J. Cosmol. Astropart. Phys. 02 (2023) 011.
[73] T. Callister, L. Sammut, S. Qiu, I. Mandel, and E. Thrane, The Limits of Astrophysics with Gravitational-Wave Backgrounds, Phys. Rev. X **6**, 031018 (2016).
[74] R. Jinno and M. Takimoto, Gravitational waves from bubble collisions: An analytic derivation, Phys. Rev. D **95**, 024009 (2017).
[75] M. Hindmarsh, S. J. Huber, K. Rummukainen, and D. J. Weir, Gravitational Waves from the Sound of a First Order Phase Transition, Phys. Rev. Lett. **112**, 041301 (2014).
[76] M. Hindmarsh, S. J. Huber, K. Rummukainen, and D. J. Weir, Numerical simulations of acoustically generated gravitational waves at a first order phase transition, Phys. Rev. D **92**, 123009 (2015).
[77] M. Hindmarsh, S. J. Huber, K. Rummukainen, and D. J. Weir, Shape of the acoustic gravitational wave power spectrum from a first order phase transition, Phys. Rev. D **96**, 103520 (2017); **101**, 089902(E) (2020).
[78] M. Hindmarsh, Sound Shell Model for Acoustic Gravitational Wave Production at a First-Order Phase Transition in the Early Universe, Phys. Rev. Lett. **120**, 071301 (2018).
[79] M. Hindmarsh and M. Hijazi, Gravitational waves from first order cosmological phase transitions in the sound shell model, J. Cosmol. Astropart. Phys. 12 (2019) 062.
[80] R.-G. Cai, S.-J. Wang, and Z.-Y. Yuwen, Hydrodynamic sound shell model, Phys. Rev. D **108**, L021502 (2023).
[81] V. Mandic, E. Thrane, S. Giampanis, and T. Regimbau, Parameter Estimation in Searches for the Stochastic Gravitational-Wave Background, Phys. Rev. Lett. **109**, 171102 (2012).
[82] T. Callister, A. S. Biscoveanu, N. Christensen, M. Isi, A. Matas, O. Minazzoli, T. Regimbau, M. Sakellariadou, J. Tasson, and E. Thrane, Polarization-Based Tests of Gravity with the Stochastic Gravitational-Wave Background, Phys. Rev. X **7**, 041058 (2017).
[83] P. M. Meyers, K. Martinovic, N. Christensen, and M. Sakellariadou, Detecting a stochastic gravitational-wave background in the presence of correlated magnetic noise, Phys. Rev. D **102**, 102005 (2020).
[84] A. Matas and J. D. Romano, Frequentist versus Bayesian analyses: Cross-correlation as an approximate sufficient statistic for LIGO-Virgo stochastic background searches, Phys. Rev. D **103**, 062003 (2021).
[85] B. Allen and J. D. Romano, Detecting a stochastic background of gravitational radiation: Signal processing strategies and sensitivities, Phys. Rev. D **59**, 102001 (1999).
[86] L. Sun *et al.*, Characterization of systematic error in Advanced LIGO calibration, Classical Quantum Gravity **37**, 225008 (2020).
[87] J. T. Whelan, E. L. Robinson, J. D. Romano, and E. H. Thrane, Treatment of calibration uncertainty in multi-baseline cross-correlation searches for gravitational waves, J. Phys. Conf. Ser. **484**, 012027 (2014).
[88] E. Thrane, N. Christensen, and R. Schofield, Correlated magnetic noise in global networks of gravitational-wave interferometers: Observations and implications, Phys. Rev. D **87**, 123009 (2013).
[89] M. W. Coughlin *et al.*, Measurement and subtraction of Schumann resonances at gravitational-wave interferometers, Phys. Rev. D **97**, 102007 (2018).
[90] J. S. Speagle, DYNESTY: A dynamic nested sampling package for estimating Bayesian posteriors and evidences, Mon. Not. R. Astron. Soc. **493**, 3132 (2020).
[91] G. Ashton *et al.*, Bilby: A user-friendly Bayesian inference library for gravitational-wave astronomy, Astrophys. J. Suppl. Ser. **241**, 27 (2019).
[92] A. Kosowsky and M. S. Turner, Gravitational radiation from colliding vacuum bubbles: Envelope approximation to many bubble collisions, Phys. Rev. D **47**, 4372 (1993).
[93] A. Kosowsky, M. S. Turner, and R. Watkins, Gravitational Waves from First Order Cosmological Phase Transitions, Phys. Rev. Lett. **69**, 2026 (1992).
[94] S. J. Huber and T. Konstandin, Gravitational wave production by collisions: More bubbles, J. Cosmol. Astropart. Phys. 09 (2008) 022.
[95] D. J. Weir, Revisiting the envelope approximation: Gravitational waves from bubble collisions, Phys. Rev. D **93**, 124037 (2016).
[96] D. Cutting, M. Hindmarsh, and D. J. Weir, Gravitational waves from vacuum first-order phase transitions: From the envelope to the lattice, Phys. Rev. D **97**, 123513 (2018).
[97] D. Cutting, E. G. Escartin, M. Hindmarsh, and D. J. Weir, Gravitational waves from vacuum first order phase transitions II: From thin to thick walls, Phys. Rev. D **103**, 023531 (2021).
[98] O. Gould, S. Sukuvaara, and D. Weir, Vacuum bubble collisions: From microphysics to gravitational waves, Phys. Rev. D **104**, 075039 (2021).
[99] D. Cutting, M. Hindmarsh, and D. J. Weir, Vorticity, Kinetic Energy, and Suppressed Gravitational Wave Production in Strong First Order Phase Transitions, Phys. Rev. Lett. **125**, 021302 (2020).
[100] J. R. Espinosa, T. Konstandin, J. M. No, and G. Servant, Energy budget of cosmological first-order phase transitions, J. Cosmol. Astropart. Phys. 06 (2010) 028.
[101] S.-J. Wang and Z.-Y. Yuwen, The energy budget of cosmological first-order phase transitions beyond the bag equation of state, J. Cosmol. Astropart. Phys. 10 (2022) 047.
[102] F. Giese, T. Konstandin, and J. van de Vis, Model-independent energy budget of cosmological first-order phase transitions—A sound argument to go beyond the bag model, J. Cosmol. Astropart. Phys. 07 (2020) 057.
[103] F. Giese, T. Konstandin, K. Schmitz, and J. van de Vis, Model-independent energy budget for LISA, J. Cosmol. Astropart. Phys. 01 (2021) 072.
[104] X. Wang, F. P. Huang, and X. Zhang, Energy budget and the gravitational wave spectra beyond the bag model, Phys. Rev. D **103**, 103520 (2021).
[105] H.-K. Guo, K. Sinha, D. Vagie, and G. White, Phase transitions in an expanding universe: Stochastic gravitational waves in standard and non-standard histories, J. Cosmol. Astropart. Phys. 01 (2021) 001.

[106] D. J. Weir, Gravitational waves from a first order electroweak phase transition: A brief review, Phil. Trans. R. Soc. A **376**, 20170126 (2018).

[107] X. Wang, F. P. Huang, and X. Zhang, Phase transition dynamics and gravitational wave spectra of strong first-order phase transition in supercooled universe, J. Cosmol. Astropart. Phys. 05 (2020) 045.

[108] R.-G. Cai, M. Sasaki, and S.-J. Wang, The gravitational waves from the first-order phase transition with a dimension-six operator, J. Cosmol. Astropart. Phys. 08 (2017) 004.

[109] J. Ellis, M. Lewicki, and J. M. No, On the maximal strength of a first-order electroweak phase transition and its gravitational wave signal, J. Cosmol. Astropart. Phys. 04 (2019) 003.